PHYSICAL REVIEW B VOLUME 56, NUMBER 24 15 DECEMBER 1997-II

Local charge injection in STM as a mechanism for imaging with anomalously high corrugation

D. Drakova* and G. Doyen
Institut für Physikalische Chemie, Ludwig-Maximilians-Universität, München, Germany
(Received 10 March 1997; revised manuscript received 4 August 1997)

The corrugation amplitude found experimentally in scanning tunnel microscopy (STM) on Al(111) is much larger than the corrugation of the charge density at the position of the tip. The experimental results on Al(111) demonstrate that the presently available interpretations of STM imaging of this surface are not consistent. We present a many-body theory that offers an explanation of the experimental data. We suggest that due to the dynamic response in the metal, the $3p_z$ affinity level gains weight near the Fermi level and by this mechanism electron injection into $3p_z$-like affinity resonances localized on the Al surface atoms becomes dominating in the tunneling process. STM images essentially show the topography of these resonances.
[S0163-1829(97)51844-3]

A long lasting puzzle of scanning tunnel microscopy (STM) on metal surfaces has been the problem of where does the corrugation of the constant current contours arise from. The corrugation on Al(111) is a major issue in theoretical STM calculations, since parallel to the surface the electron charge distribution is flat and topographically this is a densely packed surface. Furthermore, there are no surface states and resonances close to the Fermi level that might give rise to large corrugation. We suggest a many-particle approach for the solution of this problem. In the present contribution we consider the process of local electron injection and calculate the response of the metal sample surface to the locally injected electron within a many-body theory.

Our investigation reveals that a many-body treatment of the local injection process has important consequences for the corrugation amplitude observed in STM imaging. We calculate the lateral variation of the tunnel current in STM on Al(111) and find a strong enhancement of the corrugation amplitude compared to mean-field estimates. Ever since the publication of the STM imaging results on Al(111) by Wintterlin *et al.*[1] the anomalously large corrugation found in these experiments has been puzzling. Explanations have been published by various groups,[2–5] but all these suggestions can be refuted by analyzing the experiments which have been performed since then. Chen[2] concluded from a perturbation theoretical approach that W-d_{z^2} tip orbitals might give a large corrugation. From the tip preparation used in these experiments it is, however, clear that an Al atom or a cluster of Al atoms is situated at the apex of the tip.[1,6] Also the force gradients measured by Dürig and Züger[7] can only be understood theoretically, if it is assumed that the apex of the tip consists of an Al atom.[8,9] Hence, the possibility that a W atom could be at the end of the tip in these experiments can safely be excluded. Tekman and Ciraci[3] make tip-induced states responsible for the large corrugation. These tip-induced states should, however, be visible in STS which is not the case.[6] In addition, tip-induced states are predicted only for very small tip-sample separations ($\leqslant$2.5 Å) where the tunnel current would be much larger than that used in the experiments. Tseng and Tsong[4] suggest resonance tunneling as explanation and assume that a contamination between tip and sample should mediate the resonance tunneling. The experimentalists consider it, however, extremely unlikely that for the large number of measurements there should always be in a reproducible way a contamination on the tip. Also the resonance state should most probably be visible in STS. Jackobsen *et al.*[5] suggest that the STM height corrugation on Al(111) arises due to dominating tunneling via atomic p-type orbitals on the tip. The density of states in the vicinity of the Fermi level of a nonperturbed Al(111) seven-layer slab proved more strongly corrugated when it is projected on a p-tip orbital than on a s-tip orbital. However, at tip-sample separations of 2–3 Å, where the calculations in Ref. 5 have been performed, tip-sample interaction, which is not accounted for in Ref. 5, would lead to a completely new electronic structure of the combined tip+sample system, and local charge-density arguments are not relevant at such small tip-sample separations. The experiments, on the other hand, demonstrate that the large corrugation amplitude persists over a large range of the relative tip-sample distance of 2 Å for situations far from contact.

Quantitative calculations in the layer Korringa-Kohn-Rostoker formalism going beyond perturbation theory gave the result that the corrugation on Al(111) seen in STM should not be significantly larger than the corrugation of the charge density,[10] in clear discrepancy with the experimental findings.

We start from the following Hamiltonian:

$$H = H_{\mathrm{tip}} + H_{\mathrm{atom}} + H_{\mathrm{jellium}} + H_{\mathrm{int}}, \tag{1}$$

where H_{tip} is the Hamiltonian for the tip including the interaction with the sample, H_{jellium} is the Hamiltonian for a flat metal surface without atomic structure, and H_{atom} describes metal atoms in the sample surface that are embedded by means of the interaction H_{int} into the jellium background;

$$H_{\text{atom}}=\sum_{A,s}\langle As|T+V_{\text{atom}}|As\rangle n_{As}+\sum_{B,t>A,s}\langle AsBt|V_{\text{el-el}}|AsBt\rangle n_{As}n_{Bt}, \tag{2}$$

$$\begin{aligned}H_{\text{int}}=&\sum_{A,k,s}[\langle As|T+V_{\text{atom}}+V_{\text{met}}|ks\rangle a_{As}^{+}a_{ks}+\text{H.c.}]+\sum_{A,B,k,s}[\langle AsBs|V_{\text{el-el}}|Asks\rangle n_{As}a_{Bs}^{+}a_{ks}+\text{H.c.}]\\&+\sum_{A,s}^{l,t\geq k,t}[\langle Askt|V_{\text{el-el}}|Aslt\rangle n_{As}a_{kt}^{+}a_{lt}+\text{H.c.}]+\sum_{A,B}^{k,l,s,t}[\langle AsBt|V_{\text{el-el}}|kslt\rangle a_{As}^{+}a_{Bt}^{+}a_{ks}a_{lt}+\text{H.c.}]\\&+\sum_{A,k,s,t}^{m,t\geq l,t}[\langle Aslt|V_{\text{el-el}}|ksmt\rangle a_{As}^{+}a_{lt}^{+}a_{ks}a_{mt}+\text{H.c.}]+H_{\text{im}}+V_{\text{core-core}}-Q^{2}V_{\text{im}}(R_z).\end{aligned} \tag{3}$$

A, B label affinity orbitals for the metal atoms, k, l, m, n indicate eigenfunctions of H_{jellium}, s, t are spin indices, a_{is}^{+}, a_{jt} are electron creation and annihilation operators defining the number operator $n_{is}=a_{is}^{+}a_{is}$. T is the kinetic energy, V_{atom} indicates the core potentials of the metal atoms, V_{met} is the potential of the positive metal background, and $V_{\text{el-el}}$ is the electron-electron repulsion. We use this Hamiltonian to describe eight Al atoms in the first layer of the Al(111) surface embedded in jellium. The technique of embedding atoms in a Sommerfeld solid was developed earlier and is described in Ref. 11. The procedure is mathematically exact. The physical picture behind it is to make maximal use of the basis set of the embedded atoms in the area of the indented solid for the description of the electronic structure of the solid. The eight embedded Al atoms lie in the first atomic plane and they are situated 3+3+2 atoms in rows. The choice of this cluster was subject to the requirement to provide different lateral positions of the tip and not to describe the hexagonal symmetry of the surface. The embedded Al atoms are represented by $3p_z$-affinity orbitals [the affinity energy is 0.441 eV for the $3s^2 3p^2(^3P)$ gas phase negative-ion state].[12] The interaction between $3p_z$-affinity orbitals on different lattice sites is neglected; $3p_z$-affinity orbitals on different lattice sites are, however, orthogonalized. H_{tip} is not specified further as tip-sample interaction is neglected in the many-body calculations, i.e., it is treated in perturbation theory. The tip consists of an atom adsorbed on jellium and is represented by an Al $3s$ orbital. $V_{\text{core-core}}$ is the core-core repulsion, $-Q^2V_{\text{im}}(R_z)$ represents the core image energy, Q is the core charge of the embedded atoms. H_{im} describes the coupling of the affinity electrons to the plasmons and is described in detail in Ref. 13. It contains the long-range polarization of the metal due to the perturbation and includes image effects.

In an earlier study of a single Al atom adsorbed on the Al(111) and W(110) surfaces, serving as tip base, we showed that upon chemisorption the Al atom loses its $3p$ electron into the metal Fermi sea.[8,14] Hence, the $3s$ orbital is the one with significant spectral weight at E_F, which is most extensively made use of in the tunneling process. Using jellium as a tip atom base in the present study simulates the jelliumlike Al(111) surface and in addition aims at reducing the effects due to the electronic structure of the tip. As discussed above, tip-induced effects can be discarded as causing the large corrugation amplitude in the STM experiments on Al(111).

The Hamiltonian contains a detailed description of electron-electron interaction. The model we are using has been extensively described.[8,15] It was successfully applied to the study of numerous surface phenomena ranging from the mechanism of metastable quenching spectroscopy on adsorbate covered surfaces[15] to the study of atom transfer in STM, its driving forces, and consequences for STM imaging.[8,14] The role of many-particle effects in these phenomena has been explicitly analyzed. The approximations made are described in detail in Ref. 16. The work of Koetter, Drakova, and Doyen[8] demonstrates that they yield excellent results for the binding energies, equilibrium distances, tip-sample interaction energies, and forces. The matrix elements appearing in the Hamiltonians (2) and (3) are taken from this work.

We define localized jellium states by

$$|A\mu s\rangle=\frac{1}{|\langle As|A\mu s\rangle|}\sum_{l\epsilon\mu}\langle ls|As\rangle|ls\rangle. \tag{4}$$

The sum is over all jellium states $|l\rangle$ which lie within an energy range indicated by μ. In this way we introduce a discretization of the energy continuum. The states $\{|A\mu s\rangle\}$ together with the metal orbitals $|As\rangle$ form the local complex. The spatial region covered by these states is called the local region. Dyson's equation is used to couple the local complex to the continuum of jellium states.

Figure 1 illustrates the Hamiltonian and displays the physics of the charge injection process in a schematic manner. Tunneling from occupied sample states is just the time-reversed process of electron injection. The electron has to localize for a very short period of time in the affinity orbital in order to tunnel to the tip atom. It has been estimated that the tunneling process takes place within 10^{-15} sec or less (see, for example, Refs. 17 and 18 and the references therein). A hole, i.e., a positive charge, is therefore created in the local region of the affinity orbital to which the environment responds dynamically. Formally, this is just equivalent to injecting a localized hole into the sample.

The tunnel current $\mathbf{J}$ in the energy interval from E_1 to E_2 is evaluated from the Green function $\tilde{G}^{\pm}(E)$ and the potential V induced by the tip atom which is contained in H_{tip}:

$$\begin{aligned}\frac{\hbar\mathbf{J}}{2\pi e}=&\int_{E_1}^{E_2}dE\ \text{Tr}\langle\mu|\tilde{T}^{-}(E)|\nu\rangle\langle\nu|\text{Im}\tilde{D}^{\text{fin}}(E)|\lambda\rangle\\&\times\langle\lambda|\tilde{T}^{+}(E)|\kappa\rangle\langle\kappa|\text{Im}\tilde{D}^{ini}(E)|\mu\rangle,\end{aligned} \tag{5}$$

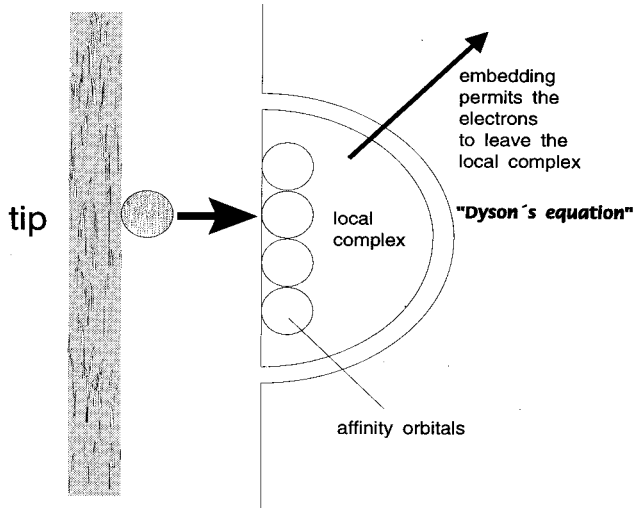

FIG. 1. Schematic illustration of the Hamiltonian and the charge injection process.

where $\langle\mu|\tilde{T}^{\pm}(E)|\nu\rangle=\langle\mu|V+V\tilde{G}^{\pm}(E)V|\nu\rangle$. The potential V is also provided by the work of Koetter, Drakova, and Doyen.[8] The set of states $\{|\mu\rangle\}$ comprises the affinity orbitals $\{|As\rangle\}$ and the states $\{|A\mu s\rangle\}$ defined in Eq. (4) and spans the Hilbert space in the local complex indicated in Fig. 1. The functions $\tilde{D}^{ini}(E)$ and $\tilde{D}^{\text{fin}}(E)$ describe the injection into and the escape out of the localized region, respectively, of the charge. $\tilde{T}^{\pm}(E)$ is the T matrix. Tr indicates summation over all states $|\mu\rangle$, $|\nu\rangle$, $|\lambda\rangle$, and $|k\rangle$. The Green function describes the behavior of the system, if an electron is added or removed from the system. If the calculation is in the mean-field approximation, the polarization of the system in response to the added or removed electron is not taken into account. We improve on this by calculating the states with the added or removed electron self-consistently with the virtual excitation of plasmons and the polarization in the environment of the injected electron taken into account. The Green function for an affinity orbital is then constructed with the help of the Lehmann representation

$$\tilde{G}_A^{+}(E)=\lim_{\eta\to 0}\left[\frac{|\langle N-1|a_A|N\rangle|^2}{E-i\eta-(E_N-E_{N-1})}+\frac{|\langle N+1|a_A^{+}|N\rangle|^2}{E+i\eta-(E_{N+1}-E_N)}\right], \tag{6}$$

and is afterwards coupled to the continuum by using Dyson's equation. $|N\rangle$ is the many-particle wave function of the ground state, $|N\pm 1\rangle$ are states with one added or removed electron, and E_N, $E_{N\pm 1}$ are the corresponding total energies. $|N\rangle$ and $|N\pm 1\rangle$ are calculated self-consistently in separate calculations, i.e., $\tilde{G}_A^{+}$ is evaluated in a ΔSCF approximation.

In Fig. 2 the calculated corrugation in comparison to experiment is shown, if the tunnel current is evaluated in the mean-field approximation.[9] (In this calculation the tip-sample interaction was explicitly taken into account.) In the mean-field approximation corrugation is only obtained for tunnel resistances that are two orders of magnitude smaller than applied in the experiments. In order to describe the dynamic process of charge injection the Hamiltonian has to be solved in a dynamic approximation as described above going beyond mean-field theory.

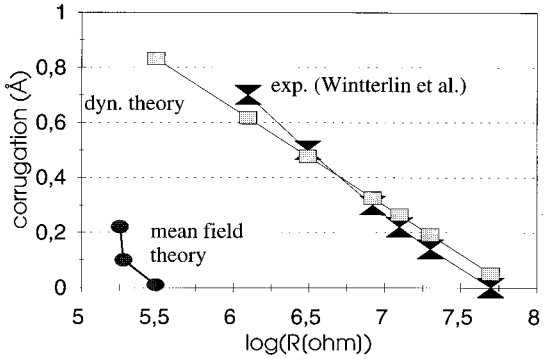

FIG. 2. STM corrugation amplitude vs tunnel resistance for Al(111).

In Fig. 3(a) we compare the spectral distribution of the affinity orbital in the mean-field and in the dynamic approximation. Compared to the mean-field results the $3p_z$-affinity level relaxes by 2.6 eV, 1.7 eV are due to the long-range polarization described by H_{im} and 0.9 eV are due to the local relaxation, i.e., the electron rearrangement within the local complex. Figure 3(b) shows an amplification of the spectral weight near the Fermi level. Compared to the mean-field situation the spectral weight of the affinity orbital near the Fermi level has increased by one order of magnitude. This means that the tunnel current will now predominantly flow

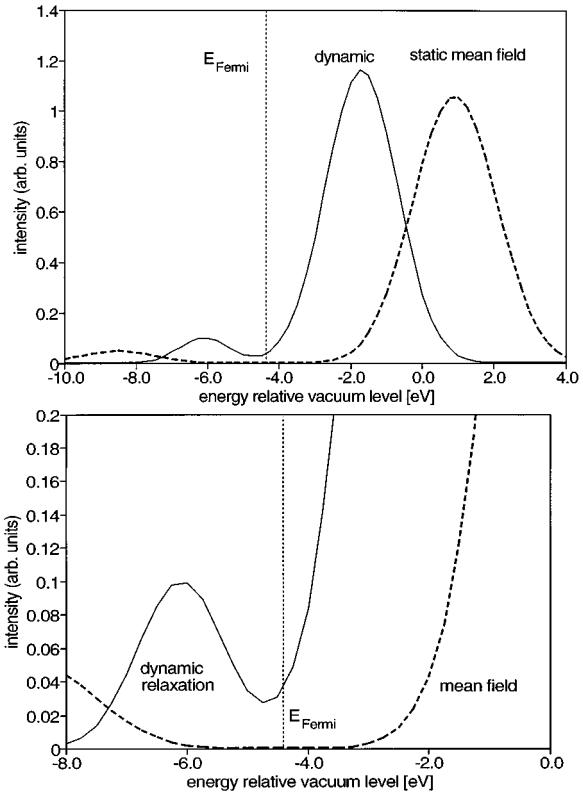

FIG. 3. Spectral distribution of the affinity orbital in the mean field and in the dynamic approximation.

via the affinity orbitals. The result on the corrugation amplitude is shown in Fig. 2. Reasonable agreement with experiment is now obtained. The enhanced corrugation amplitude is due to the fact that the charge injection occurs in a relatively localized region. The probability for charge injection into the affinity orbital varies laterally, being largest on top of the Al atoms. This results in a variation of the tunnel current with the lateral tip position.

The local nature of charge injection in STM and the dynamic relaxation lead to enhancement of the spectral weight of the surface affinity resonance at E_F and hence to increased tunneling current. This effect is more pronounced with the tip above a sample atom because the probability for electron injection in the affinity resonance is higher. It is well known that affinity levels shift towards lower energy when the interaction with the image potential is accounted for. Our conclusion does not involve the peculiarities of the method and the model used. It is simply a consequence of accounting for the response of the surrounding medium to the presence of the injected charge. Any method including the many-body response (cf., e.g., Ref. 19) could be used to check our results. Varying parameters or relaxing approximations, if subject to the constraint of describing the correct physical behavior, will not change the conclusion about the origin of the high corrugation amplitude in STM on Al(111).

An interesting feature is the nearly linear dependence of the corrugation amplitude on the logarithm of the tunnel resistance over the considered distance range, which is found both in our theory and in experiment, but which is not obtained for instance in Chen's attempt.[2] The explanation is that the distance range displayed in Fig. 2 is in the linear part of the S-shaped curve near the point of inflection. Nearer to the surface the increase of the corrugation amplitude slows down because the $3p_z$ orbital has a node at the position of the Al atom. Nearer to the surface the relative weight of tunneling via the uncorrugated Bloch states increases and therefore the corrugation amplitude does not continue to increase exponentially with distance.

Concluding, we presented a dynamical theory of STM that takes into account the image interaction and local relaxation effects in the metal. The inclusion of the dynamic relaxation in response to the local electron injection process leads to significant relaxation of the surface affinity resonances towards the Fermi level. This results in an enhancement of their spectral weight at E_F and favors the dominance of tunneling via the surface affinity states. The Hamiltonian was solved in a mean-field approximation and in a higher dynamic approximation. The mean-field solution yields a small corrugation amplitude characteristic of the ground-state charge density, whereas the dynamic approximation results in a significantly increased corrugation for values of the tunnel current, which correspond to the experimental situation. Within the dynamical theory we come to the conclusion that STM on Al(111) images the topography of the relatively localized surface affinity resonance states. This represents the physical background for the high constant height corrugation amplitude on the Al(111) surface.

---

*Permanent address: University of Sofia, Sofia, Bulgaria.

[1] J. Wintterlin, J. Wiechers, H. Brune, T. Gritsch, H. Höfer, and R. J. Behm, Phys. Rev. Lett. **62**, 59 (1989).

[2] J. C. Chen, Phys. Rev. Lett. **65**, 448 (1990).

[3] E. Tekman and S. Ciraci, Phys. Rev. B **42**, 1860 (1990).

[4] N. J. Tseng and I. S. T. Tsong, Phys. Rev. B **41**, 2671 (1990).

[5] J. Jacobsen, B. Hammer, K. W. Jacobsen, and J. K. Norskov, Phys. Rev. B **52**, 14 954 (1995).

[6] H. Brune, Ph.D. thesis, Free University of Berlin, 1992.

[7] U. Dürig and O. Zünger, Vacuum **41**, 382 (1990).

[8] E. Koetter, D. Drakova, and G. Doyen, Phys. Rev. B **53**, 16 595 (1996).

[9] E. Koetter, Ph.D. thesis, Technische Universität Berlin, 1992.

[10] G. Doyen, D. Drakova, and M. Scheffler, Phys. Rev. B **47**, 9778 (1993).

[11] G. Doyen and D. Drakova, Surf. Sci. **178**, 375 (1986).

[12] A. A. Radzig and B. M. Smirnov, *Reference Data on Atoms, Molecules and Ions* (Springer, Berlin, 1985).

[13] M. E. Grillo, G. R. Castro, and G. Doyen, J. Phys.: Condens. Matter **4**, 5103 (1992).

[14] E. Koetter, D. Drakova, and G. Doyen, Surf. Sci. **331-333**, 679 (1995).

[15] D. Drakova and G. Doyen, Phys. Rev. B **50**, 4701 (1994).

[16] D. Drakova, G. Doyen, and R. Hübner, J. Chem. Phys. **89**, 1725 (1988).

[17] K. L. Sebastian and G. Doyen, Phys. Rev. B **47**, 7634 (1993).

[18] D. Drakova and G. Doyen, Surf. Sci. **226**, 263 (1990); G. Doyen and D. Drakova, in *Quantum Chemistry Approaches to Chemisorption and Heterogeneous Catalysis,* edited by F. Ruette (Kluwer, Dordrecht, 1992), p. 139.

[19] A. Martin-Rodero, F. Flores, M. Baldo, and R. Pucci, Solid State Commun. **44**, 911 (1982).